

Direct observation of Feshbach enhanced s -wave scattering of fermions

D Genkina¹, LM Aycock^{1,2}, BK Stuhl¹, H-I Lu¹ and IB Spielman¹[‡]

¹Joint Quantum Institute, National Institute of Standards and Technology, and University of Maryland, Gaithersburg, MD, 20899 USA

²Physics Department, Cornell University, Ithaca, NY 14850 USA

E-mail: ian.spielman@nist.gov

Abstract. We directly measured the s -wave scattering cross-section of ^{40}K atoms across a Feshbach resonance. We collided a pair of degenerate clouds and imaged the scattered atoms. Owing to their low density, few atoms scattered, even near the resonance. To optimize signal to noise, we develop techniques to interpret absorption imaging in the regime where the optical intensity changes dramatically as light traverses the cloud, and recoil induced detuning corrections are significant. We applied these techniques to our s -wave scattering data and extracted the resonant magnetic field value. These imaging techniques are generally applicable, and can be used to observe effective p -wave scattering in the presence of spin-orbit coupling in a spin polarized Fermi gas.

Keywords: Quantum gases, Atomic physics

[‡] Corresponding author

1. Introduction

Feshbach resonances are a stand-by technique for tuning the interaction strength in ultracold atomic gases. Even weak interactions play a crucial role in the physics of atomic Bose-Einstein Condensates (BECs), giving rise to, for example, their characteristic Thomas-Fermi density profiles. The effects of interactions in Fermi gases, however, are harder to observe. The density of Fermi clouds is typically reduced by a factor of 10^3 from that of BECs, making it necessary to enhance the strength of interactions in order to observe them. Feshbach resonances alter the inter-atomic scattering length via the magnetic field. Not only do they enable detection of interactions, but they make it possible to tune interactions from attractive to repulsive, allowing for the phase transition from the BCS to BEC regime at sufficiently low temperatures [8].

A Feshbach resonance occurs when a bound molecular state of few atoms energetically approaches the free atomic state [1]. The energy of the atomic states is defined by their hyperfine state and tunable with a bias magnetic field. The Feshbach resonance can thus be approached by changing the bias field. The effect of the resonance on the scattering length between two free atoms in the appropriate hyperfine states is

$$a(B) = a_{bg} \left(1 - \frac{\Delta}{B - B_0} \right), \quad (1)$$

where a is the scattering length, a_{bg} is the scattering length away from the resonance, Δ is the width of the resonance, and B_0 is the field value at which the resonance occurs. Note that the scattering length tends to infinity from either side of the resonance.

To use Feshbach resonances as a tool it is necessary to have a good measurement of the parameters in the above equation. The exact value of the resonant field value B_0 is impossible to calculate analytically and must be estimated via numerical models [2,4] or determined experimentally. Some experimental techniques that have been used to characterize Feshbach resonances include: the observation of loss due to three-body inelastic scattering, re-thermalization timescales, or anisotropic expansion, all of which infer the elastic scattering cross section from collective behavior of the cloud [5–7].

Here we present a new technique for measuring the location and width of a Feshbach resonance. We collide a pair of ultra-cold Fermi gases and directly image the resulting s -wave scattering halo as a function magnetic field strength. This allows us to observe the enhancement in scattering without relying on proxy effects. We measured the fraction of atoms scattered during the collision, and from this fraction deduced the resonant magnetic field and width of the resonance.

Our Fermi gases are so dilute that even with the resonant enhancement of the scattering cross section, only a small fraction of the atoms scatter. This makes direct detection of s -wave scattering halos difficult due to detection uncertainty, which disproportionately affects regions of low atomic density. To optimize the signal to noise for low atom numbers, we utilized a non standard imaging regime. In this regime, simulation was necessary for an accurate interpretation of the images. We performed

these simulations and used the results to extract the atom number and the scattered fraction from our images.

This paper is in two parts. In the first, we study absorption imaging in the presence of significant time-dependent Doppler shift and show how we use our results to interpret data. In the second, we describe our *s*-wave scattering experiment and extract a measure of the location of the Feshbach resonance in ^{40}K .

2. Absorption imaging in the presence of strong recoil induced detuning

Every experiment requires a detection scheme. In ultracold atomic experiments, detection relies on imaging laser light that has interacted in some way with the atomic cloud. The most common such imaging method, and the one we use in our experiments, is absorption imaging. Absorption imaging utilizes some excited to ground state transition between two levels of the atom. Such an atomic transition has an energy difference E_0 , an associated frequency $\omega_0 = E_0/\hbar$, and a natural transition linewidth Γ . When interacting with a laser light field an atom will scatter photons: it will absorb a photon from the light field and move up to its excited state, and then re-emit the photon in a random direction and decay back to its ground state. The rate at which this scattering occurs, given a laser intensity I , is given by

$$\gamma_{sc} = \frac{\Gamma}{2} \frac{I/I_{sat}}{1 + (2\delta/\Gamma)^2 + I/I_{sat}}, \quad (2)$$

where I_{sat} is the saturation intensity, the intensity at which the atom is equally likely to be in the ground and excited state, and δ is the detuning, the difference between the resonant transition frequency ω_0 and the frequency of the laser light ω_L .

To obtain an absorption image, one shines an on or near resonant probe beam ($\delta \approx 0$) onto the atomic cloud. Some of the light is scattered by the atoms, and the part of the beam that made it through the cloud is imaged onto a camera, as seen in Fig. 1a (top). Then, the atoms are allowed to leave the trap, and the probe light is shined directly at the camera to calibrate the intensity of light that the atoms saw (bottom). The intensity in the second camera image is called the initial intensity, I_0 , as it is assumed to be the same as the intensity in the first beam before interaction with atoms. The intensity in the first image is called the final intensity, I_f .

The observed intensity in the two images can be used to infer the number of atoms that the light encountered. To do this, consider what happens to the light as it travels along the imaging axis z through a column of atoms. In general, the atomic density is three dimensional, $\rho(x, y, z)$. For the purposes of this discussion, let us focus on a single pixel of the camera, and thus a single value of I_0 and I_f and a single column of atoms, $\rho(z)$. We will not be able to infer the entire atomic distribution, but for each pixel we will be able to deduce the total 2-d atomic density, $n = \int \rho(z) dz$. As the light travels through a column of atoms, each atom will scatter light according to Eq. (2). Therefore, the atoms further along the imaging axis z will see a reduced light intensity,

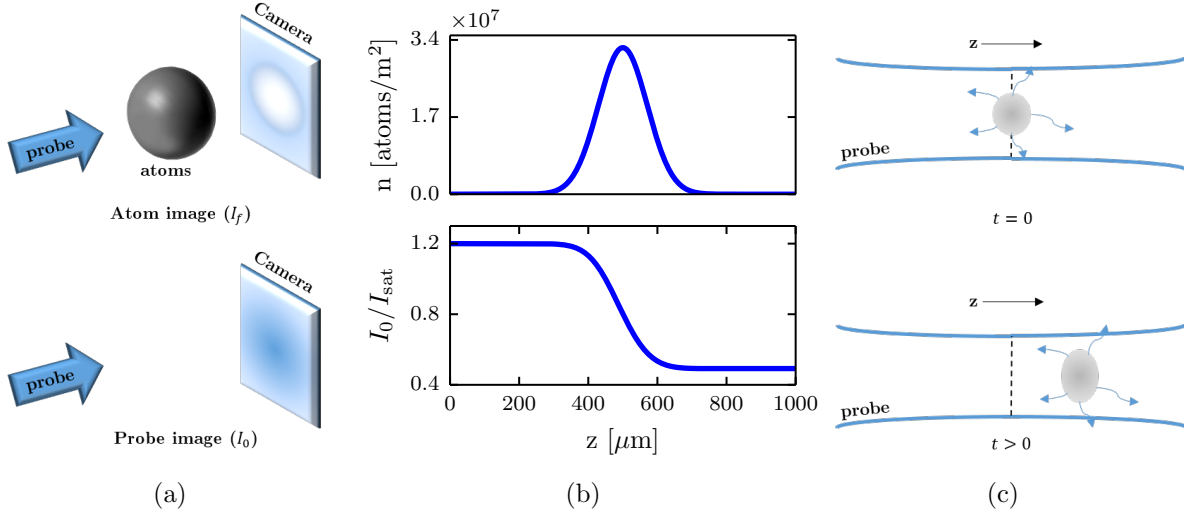


Figure 1. Absorption imaging. a. First, a near resonant probe light is shined on the atoms, and the shadow of that light is imaged on the camera. Then, the atoms are allowed to escape their trap and an image of just the probe light is taken. b. As the probe beam, travels through the atomic cloud, some of its power is absorbed, and the intensity seen by atoms further along the imaging direction z is lowered. c. An atomic cloud illuminated by a probe light field absorbs photons from the probe and re-emits them in arbitrary directions. This process results in a net velocity of the cloud in the direction of the probe light as well as diffusive spreading in the transverse directions.

as seen in Fig. 1b. The amount of light lost to scattering as a function of z is given by

$$\frac{dI(z)}{dz} = \hbar\omega_L\rho\gamma_{sc} = -\rho\sigma_0 \frac{I(z)}{1 + I(z)/I_{sat}}, \quad (3)$$

where σ_0 is the resonant scattering cross section. We have assumed $\delta = 0$. This equation can be easily integrated over z to obtain [9]

$$\sigma_0 n = -\ln\left(\frac{I_f}{I_0}\right) + \frac{I_0 - I_f}{I_{sat}}. \quad (4)$$

In the limit where the probe intensity is much smaller than the saturation intensity, $I_0 \ll I_{sat}$, this becomes simply $-\ln(I_f/I_0)$. This quantity is called the optical depth, or OD. Since this is the simplest possible model that relates the observed intensities to the column density n , we call this quantity OD_0 . Once the probe intensity becomes comparable to the saturation intensity, the second term in Eq. (4) becomes significant. We can then call this the optical density corrected for high probe intensity, or

$$OD_1 = OD_0 + \frac{I_0 - I_f}{I_{sat}}. \quad (5)$$

There are further corrections that this equation does not take into account. In particular, it neglects the atomic recoil momentum and its effect on the laser detuning, which will be discussed below.

When an atom absorbs a photon from the laser light field and gets excited to a higher energy level, by conservation of momentum it must also acquire a velocity in

the direction of the light field. This is called the recoil velocity, and it is given by $v_r = \hbar k/m$, where k is the wavenumber of the light field and m is the atomic mass. When the photon is subsequently emitted and the atom returns to its ground state, it is emitted in an arbitrary direction. Thus, the momentum lost due to emitting a photon is on average zero. The variance, however, is not zero, allowing the atoms to acquire some momentum transverse to the laser field. We will ignore this correction, but the effect of this on the atomic cloud is picture in Fig. 1c.

Once the atoms absorb enough photons, they acquire a substantial velocity in the direction of the light field, and this velocity Doppler shift them from the light field itself. Thus, an atom that absorbs N photons acquires a velocity of Nv_r and a detuning of $\delta = kNv_r$ from the probe beam. Therefore, even if the probe beam is initially on resonance with the atomic transition, we cannot neglect the detuning term in the scattering rate as time goes on. Furthermore, this detuning will vary both with imaging time t and with distance along the propagation direction z (Fig. 2). Thus, the intensity lost to the atoms also acquires a time dependence:

$$\frac{dI(t, z)}{dz} = \sigma_0 \rho \frac{I(t, z)}{1 + (2\Gamma/\delta(t, z))^2 + I(t, z)/I_{sat}}, \quad (6)$$

where the detuning δ is given by

$$\delta(t, z) = \frac{v_r}{\hbar c \rho} \int_0^t \frac{dI(z, \tau)}{dz} d\tau. \quad (7)$$

In this case, one can no longer obtain a straightforward relation between the atom number and the intensities in the two absorption images.

One can consider this equation perturbatively in time and obtain corrections to second order in imaging time, OD_2 [3]. However, the perturbative treatment breaks down shortly after the zeroth order approximation of Eq. (4) (Fig. 3). In order to adequately correct for the recoil induced detuning of the atoms, we must simulate the process and obtain numerical predictions for I_f given a certain imaging time, atomic density, and probe intensity.

In the following, we describe two versions of this simulation. First, we take the simplistic approach that the on-axis distribution of atoms does not change dramatically during the imaging time and can be treated statically. We test this approach in known limits and then check the validity of the static assumption. It turns out that, for realistic input parameters, this assumption is grossly incorrect. So, we take a slightly more sophisticated approach and allow the atoms to move within the cloud during the imaging time. This allows us to simulate the phase space evolution of atoms subjected to probe light. However, we find that while the atomic trajectories are wildly different, the predicted ODs only vary on the 0.5% level between the two models.

2.1. Stationary atom model

In order to solve eqs. [6]-[7], we start with an input 1-d distribution of atom densities $\rho(z)$, usually Gaussian in shape. We divide the cloud into spatial bins (the bin size was

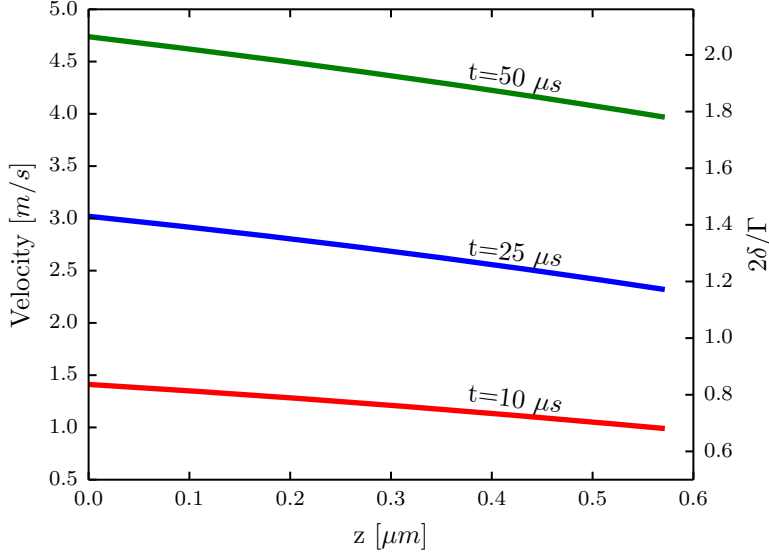


Figure 2. Distribution of generalized detuning $\Delta = \frac{2\delta}{\Gamma}$ across an atomic cloud of ^{40}K for three different imaging times, as obtained by numerical simulation.

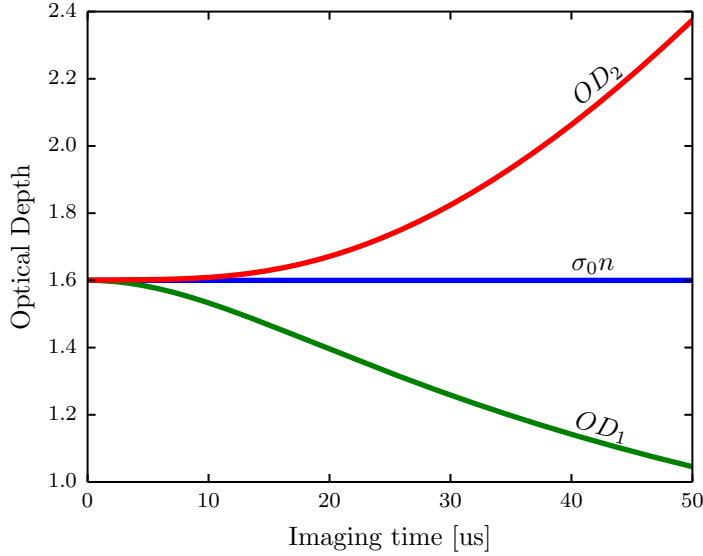


Figure 3. Using time dependent I_f values obtained from recoil detuning corrected simulation of on-resonant imaging of ^{40}K atoms, this graph shows the optical depths each model would deduce from such images. The true optical depth is given at 1.6. OD_1 is the high probe intensity corrected optical depth given by 4. OD_2 is the model that includes high probe intensity corrections and imaging time corrections from expanding 6,7 to second order in imaging time [3]. Note that the value obtained using the second order expansion in time starts to differ significantly from the true value after about 15us. The probe intensity is $0.8 I_{sat}$.

chosen such that decreasing the bin size further produced less than a 0.001% difference in the result). In this approximation, we keep the number of atoms in each bin constant. The algorithm used is shown in alg. [1]. We call the optical depth obtained from this algorithm OD_{corr1} .

Algorithm 1 Stationary atom model

```

 $I[n = 0, t] = I_0$  { $n$  is the bin index,  $t$  is the time index,  $I$  is in units of  $I_{sat}$ }
 $\delta[n, t = 0] = 0$  {light initially resonant,  $\delta$  in units of  $\Gamma/2$ }
 $I_f = 0$ 
for  $t = 0$  to  $t_f$  do {loop over time steps}
  for  $n = 1$  to  $N$  do {loop over bins,  $N$  is total bin number}
     $A = \sigma_0 \rho[n] dz$ 
     $B = v_r dt / (\hbar c \rho[n])$ 
     $I[n, t] = I[n - 1, t] - AI[n - 1, t] / (1 + \delta[n, t - 1]^2 + I[n - 1, t])$  {Eq. (6)}
     $\delta[n, t] = \delta[n, t - 1] + B(I[n - 1, t] - I[n, t])$  {Eq. (7)}
  end for
   $I_f += I[N, t] dt$ 
end for
 $OD_{corr1} = -\ln(I_f / I_0 t_f)$ 

```

To check the validity of our simulation, we can take it to certain limits in which the problem becomes analytically solvable. In the limit that the probe intensity is much weaker than saturation, $I_0 \ll I_{sat}$, the atoms will not absorb enough light to significantly detune from resonance. We can then neglect time dependence and Eq.(6) reduces to

$$\frac{dI(z)}{dz} = -\rho\sigma_0 I(z), \quad (8)$$

from which we recover the simple

$$\sigma_0 n = OD_0 = -\ln I_0 / I_f. \quad (9)$$

In the limit that the probe intensity is much stronger than saturation, $I_0 \gg I_{sat}$, even far detuned atoms will absorb light at their maximum, allowing us to again neglect the time dependence and reduce 6 to

$$\frac{dI(z)}{dz} = -\rho\sigma_0 I_{sat}, \quad (10)$$

which integrates to

$$\sigma_0 n = \frac{I_0 - I_f}{I_{sat}}. \quad (11)$$

We recognize the right hand sides of Eq. (9) and Eq. (11) as the two terms in the expression for OD_1 , Eq. (4). Thus, in both limits OD_{corr1} should coincide with the value of OD_0 obtained by fixing an input atom number n in Eq. (4). Indeed, they coincide as seen in Fig. 4.

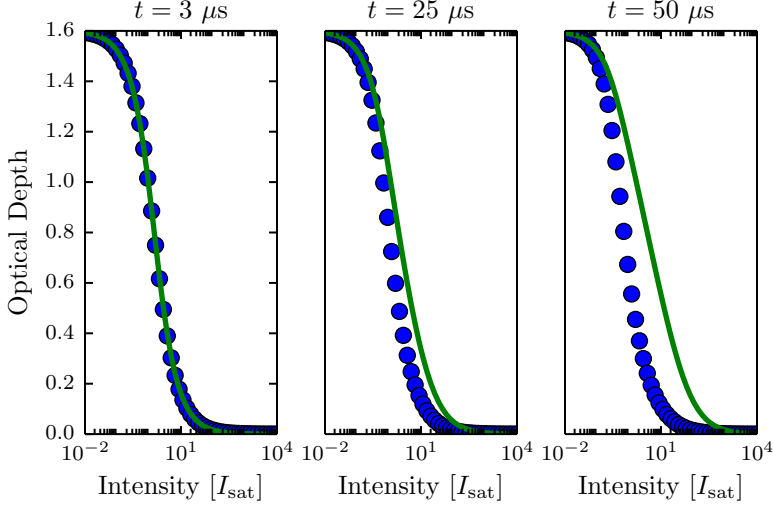


Figure 4. Optical density as a function of probe intensity as predicted by the simulation (blue dots) and by Eq. (9) (green lines), for three different imaging times. The predictions agree in both the high and low intensity limits, and differ for probe intensities comparable to the saturation intensity. The difference is enhanced with increased imaging time.

We can use the results of this simulation to check if the stationary atom assumption is self consistent, ie if the distance traveled by the atoms in one bin during the imaging time is less than the bin size. However, as can be seen from Fig. 8, it turns out that not only do the atoms travel more than the bin size, but they also travel more than the size of the whole cloud, and the back of the cloud even overtakes the front for long enough imaging times. Thus, the atomic distribution as a function of position changes dramatically during the imaging time, and our stationary assumption is completely invalid.

2.2. Traveling atom model

To account for the changing atomic distribution during the imaging pulse, we shift our framework slightly from spatial bins of equal size with varying atoms number to superatoms. These superatoms were spatially distributed to match a typical experimental distribution, each describing the aggregate behavior of N_{sa} atoms. The amended algorithm is shown in alg.[2].

First, we check the velocity behavior in this model against known limits. One such limit is that of a single superatom. In this case, there is no attenuation, and the intensity seen by the superatom is constant at I_0 . The only thing that evolves in time is the detuning of the single superatom. We can differentiate both sides of Eq. (7) to obtain

$$\frac{d\delta(t)}{dt} = \frac{v_r}{\hbar c \rho} \frac{dI}{dz}, \quad (12)$$

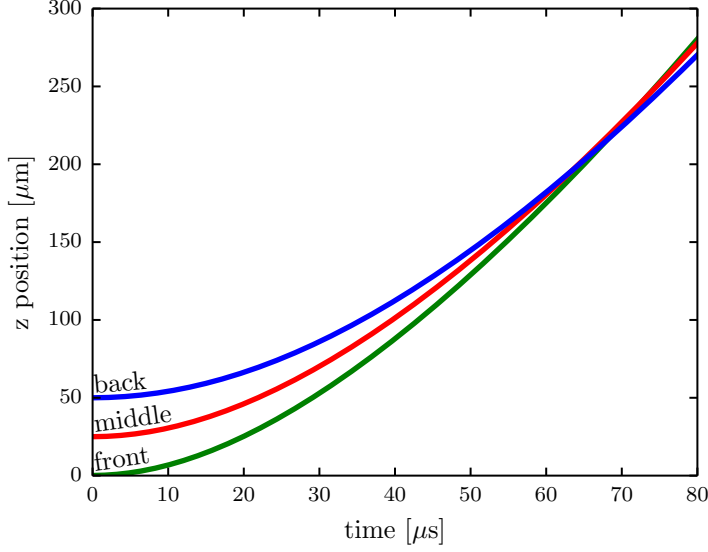


Figure 5. Position of atoms as a function of imaging time for atoms in the first, middle, and last bins of the simulation. The probe intensity here is $1.2I_{sat}$, and the optical depth is 1.6.

Algorithm 2 Travelling atom model

$S[n] = \text{Superatom}(z = z_0[n], \delta = 0)$ {initialize array of superatom class instances, with position and detuning attributes}

$I[n = 0, t] = I_0$ { t is the time index, I is in units of I_{sat} }

$I_f = 0$

for $t = 0$ to t_f **do** {loop over time steps}

for $n = 1$ to N **do** {loop over superatoms}

$A = \sigma_0 N_{sa} dz$

$B = v_r dt / (\hbar c N_{sa})$

$I[n, t] = I[n - 1, t] - AI[n - 1, t] / (1 + S[n].\delta^2 + I[n - 1, t])$ {Eq. (6)}

$S[n].\delta += B (I[n - 1, t] - I[n, t])$ {Eq. (7), detuning in units of $\Gamma/2$ }

$S[n].z += dt\Gamma\delta/2k$ { k is the wavenumber, $\Gamma\delta/2k$ is the velocity at δ detuning}

end for

$S[n] = \text{sort}(S[n], \text{key} = \text{Superatom}.z)$ {sort superatoms by current position}

$I_f += I[N, t]dt$

end for

$OD_{corr2} = -\ln(I_f/I_0 t_f)$

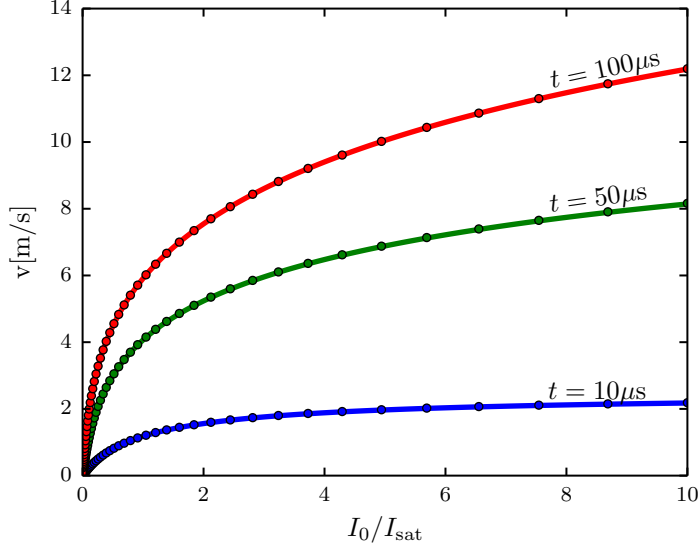


Figure 6. The velocity of a single superatom as a function of probe intensity for various imaging times. Simulation data (dots) and analytical solutions (lines) are in good agreement.

and Eq. (6) simplifies to

$$\frac{dI}{dt} = \frac{v_r \sigma_0}{\hbar c} \frac{I_0}{1 + (2\delta(t)/\Gamma)^2 + I_0/I_{\text{sat}}}. \quad (13)$$

Combining Eq. (12) and Eq. (13), and converting to a dimensionless form, we obtain

$$\frac{d\Delta(t)}{dt} = kv_r \frac{\tilde{I}}{1 + \Delta^2 + \tilde{I}}, \quad (14)$$

where $\Delta = 2\delta/\Gamma$, $\tilde{I} = I_0/I_{\text{sat}}$ and k is the photonic wavevector. Equation (14) can be solved numerically, and is in good agreement with our simulation, as seen in Fig. 6.

We use this model to study the time evolution of the cloud shape during imaging. This can be visualized as the phase space evolution of superatoms, as seen in Fig. 7. We see that the cloud shape is actually strongly distorted during the imaging time.

We compare the optical depths predicted by each of the two models, OD_{corr1} and OD_{corr2} . We find that, despite the significant changes in atomic distribution during the imaging time, the predicted optical densities are so slightly changed by including this effect that it is practically undetectable, as seen in Fig. 8. In fact, the difference $|OD_{\text{corr1}} - OD_{\text{corr2}}|/OD_{\text{corr1}} \leq 0.005$. Thus, for the purposes of deducing the atom density from experimental optical depths, simply using a stationary model is sufficient. Furthermore, the actual atomic distribution $\rho(z)$ is largely irrelevant, and the only observable is the 2-D atomic density $n = \int \rho(z) dz$.

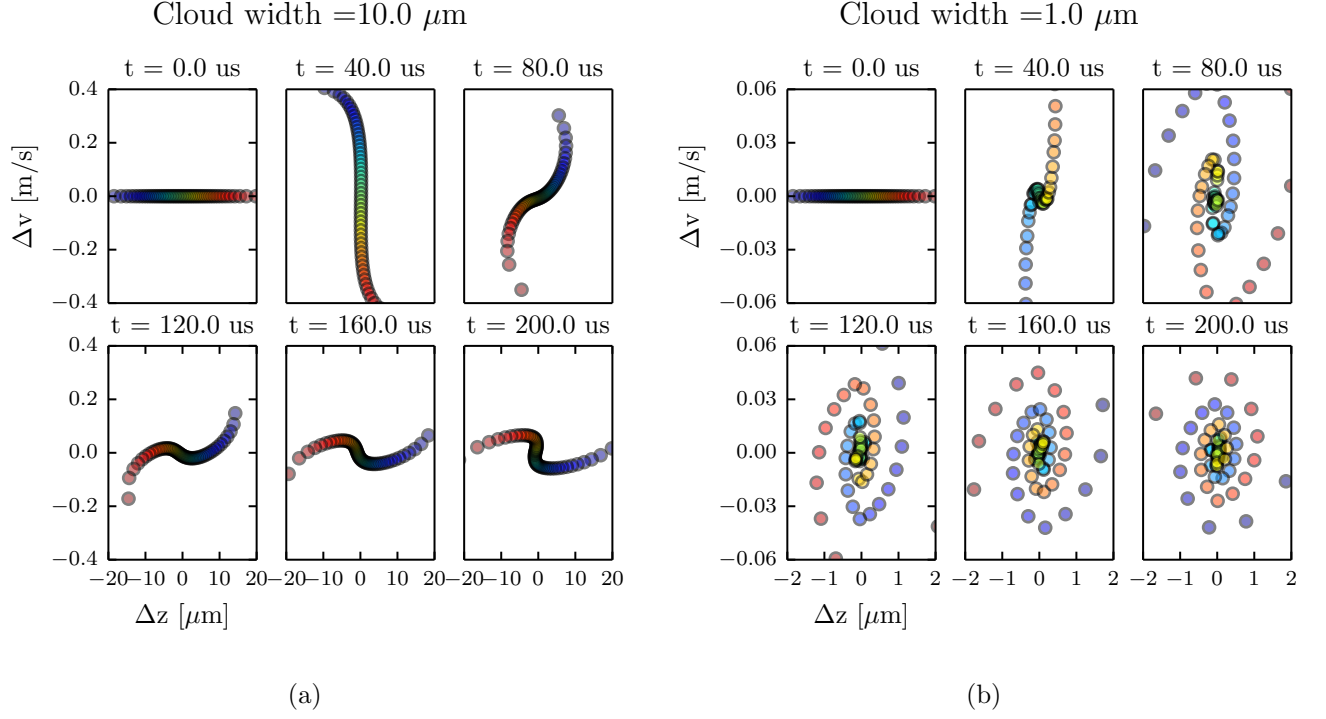


Figure 7. Phase space evolution of an atomic cloud exposed to probe light of $1.2I_{sat}$. We have used $\Delta v = v - \langle v(t) \rangle$ and $\Delta z = z - \langle z(t) \rangle$, subtracting out the center of mass position and velocity of the cloud. The optical depth is 1.6, and the initial cloud is a gaussian with width a. $10\mu\text{m}$ and b. $1\mu\text{m}$.

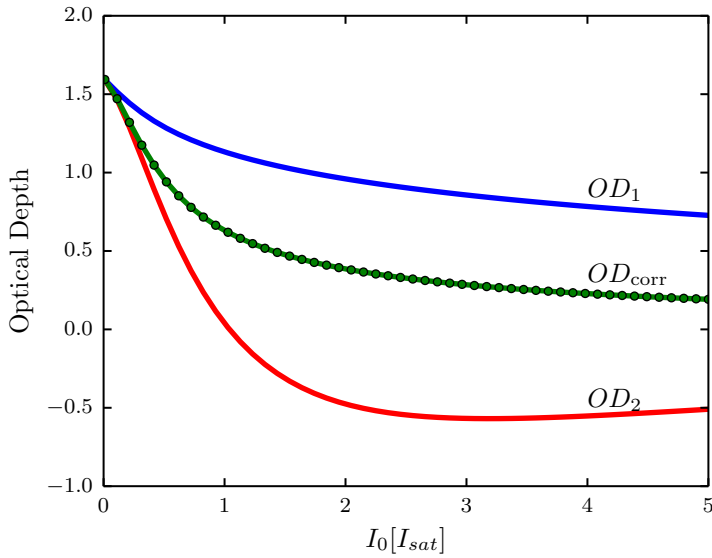


Figure 8. Predictions for optical depth as a function of probe intensity for an imaging time $t = 100\mu\text{s}$. Note that the two versions of simulated optical depth, OD_{corr1} (green line) and OD_{corr2} (green dots) are virtually indistinguishable.

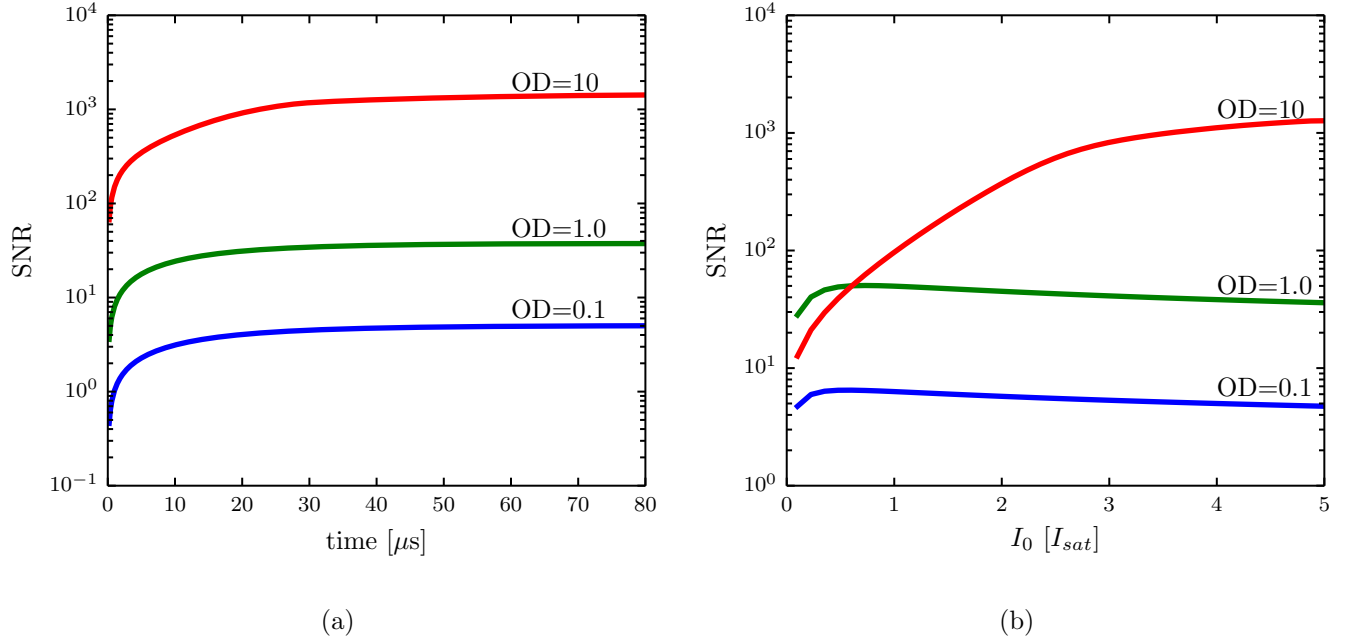


Figure 9. Signal to noise ratio (SNR) for three different optical depths after correcting for recoil induced detuning. a. SNR as a function of probe intensity $I_0/I_{\text{sat}} = 5.0$ and b. SNR as a function of probe intensity for an imaging time of $50\mu\text{s}$.

2.3. Signal to noise optimization

This simulation can be used to interpret experimentally obtained initial and final intensities. For a given imaging time, we create a look-up table of predicted optical depth as a function of probe intensity and atomic density. We can then find the observed optical depth on this table, with the given probe intensity, and infer the atomic density. The uncertainty in the measured intensities can be propagated through this procedure, and we can establish optimal imaging parameters to maximize the signal to noise ratio of this detection scheme.

Here, the only source of measurement uncertainty we consider is the photon shot noise, which is Poisson distributed and has a standard deviation proportional to $\sqrt{N_p}$, where N_p is the photon number. We then propagate this uncertainty through our correction scheme to get the uncertainty in our deduced value of $\sigma_0 n$. We define the signal to noise ratio (SNR) as $\sigma_0 n / \delta_{\sigma_0 n}$, where $\delta_{\sigma_0 n}$ is the propagated measurement uncertainty.

As seen in Fig. 9, after about $40\mu\text{s}$ extending the imaging time no longer yields appreciable improvement in signal to noise ratio. The advantage of imaging for $40\mu\text{s}$ as opposed to $10\mu\text{s}$ where the uncorrected model is appropriate is about a factor of 1.5 increase in SNR. We performed the experiments described in the second section at $40\mu\text{s}$ imaging time.

2.4. Calibration of saturation intensity

A key component of good detection is a well calibrated measurement apparatus. In this case, the measurement apparatus is a CCD camera used to take the absorption images. We used Point Grey's Flea3 camera. Each camera pixel converts the photons it is exposed to, with some efficiency, into photoelectrons, and then to a digital signal, and integer we will call the number of 'counts'. The number of photons that hit a pixel and the number of 'counts' it outputs are directly proportional. However, the proportionality constant depends on many factors, such as the quantum efficiency of the camera, the photoelectric conversion factor of the camera, and the polarization of the probe light.

The most accurate way to determine this factor is through a direct experiment. In the limit where the system is adequately described by Eq. (9), only the ratio of the initial and final intensities matters, and thus this proportionality constant is irrelevant. In all other regimes, however, the ratio of the initial and final intensities to the saturation intensity also comes into play, making the proportionality constant significant. One way to approach this calibration is to determine the value of the saturation intensity in 'counts' per unit time.

In order to calibrate the saturation intensity in camera counts per unit time, we take absorption images of a cloud of ^{40}K atoms at three different imaging times, 40us, 100us, and 200us, at varying probe intensities. We pick a small square in the center of the cloud, where the atomic density is approximately uniform, and average the initial and final intensities of each pixel in the square. Thus, for each image we obtain one I_0 and one I_f , in counts per microsecond. We then do a least squares fit of OD_{corr} , our simulated optical depth, to the data. The two fit parameters are the atomic density n at the center of the cloud and the value of I_{sat} in counts per microsecond. As seen in Fig. 10, the model produces a good fit to the experimental data, and we obtain a calibration of the saturation intensity for our experiment.

3. S-wave scattering experiment

In this section we describe our Fermi scattering experiment. We scattered two counter-propagating clouds of ^{40}K atoms and observed the resulting s -wave halo of scattered atoms. We measured the dependence of the scattered atomic fraction on the bias magnetic field in the vicinity of the Feshbach resonance. We used this data to extract the location of the magnetic fields resonance of 20.247(2) mT and a width of 1.0(1) mT.

3.1. Experimental procedure

Our cold Fermi cloud preparation was as follows. We prepared clouds of cold ^{40}K atoms in a hybrid ^{40}K and ^{87}Rb apparatus. We used a Zeeman slower to slow both species before being captured in a Magneto-Optical Trap (MOT). We allowed both species to cool in optical molasses for 2 milliseconds. Then, the ^{40}K atoms were optically pumped

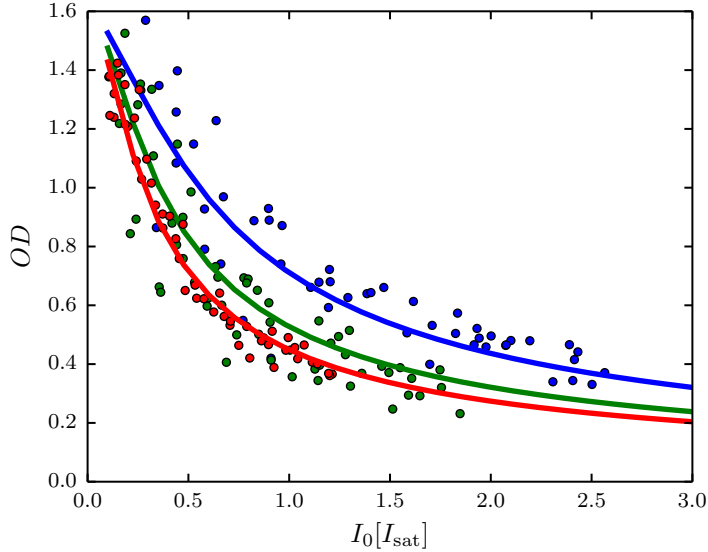


Figure 10. The optical depth as a function of probe intensity for three imaging times: $t = 40\mu\text{s}$ (blue), $t = 75\mu\text{s}$ (green), $t = 100\mu\text{s}$ (red). The dots represent experimental data and the lines represent the best fit of simulated data. The optimal fit parameters pictured are a $\sigma_0 n$ of 1.62 and saturation intensity of 29 counts/ μs .

into the magnetically trappable $|F = 9/2, m_F = 9/2\rangle$ state. Both species were then loaded into a quadrupole magnetic trap, and cooled evaporatively. Since the ^{40}K atoms only interact very weakly with each other, they only re-thermalize due to interaction with ^{87}Rb atoms, and therefore the ^{87}Rb atoms are necessary to evaporatively cool ^{40}K . We then load the atoms into a crossed optical dipole trap, with trap frequencies of 39, 42, 124 Hz in the three spatial directions [I GOT THOSE FROM ROSS'S PAPER COULD BE WRONG FOR US]. We continued evaporative cooling by slowly ramping down the dipole trap. We then used adiabatic rapid passage (ARP) to transfer the ^{87}Rb atoms from the $|F = 2, m_F = 2\rangle$ state to the $|F = 1, m_F = -1\rangle$ absolute ground state. This state was chosen to minimize spin changing collisions with ^{40}K atoms during any further evaporation. We then briefly shined an on-resonant probe light to force any remaining $F = 2$ atoms out of the trap. We again used ARP to transfer the ^{40}K atoms into an equal superposition of $|F = 9/2, m_F = -9/2\rangle$ and $|F = 9/2, m_F = -7/2\rangle$, and further evaporated in the dipole trap. The $|9/2, -9/2\rangle$ and $|9/2, -7/2\rangle$ hyperfine states of ^{40}K were then used to study their Feshbach resonance.

We then ramped the bias field in a two-step fashion to the desired value B near the Feshbach resonance. To approach the field, we used a large pair of coils in Helmholtz configuration to bring the magnetic field 0.59 mT of B . We held the atoms there to allow the eddy currents in the large coils to settle, and then used a smaller set of Helmholtz coils to hop the field the remaining 0.59 mT. We took two sets of data: one coming

from below the resonance, where we hopped the large coils to $B - 0.59mT$ and used the small coils to hop up to the desired field, and one coming from above the resonance, where we hopped the large coils to $B + 0.59mT$ and then used the small coils to hop the field down to the desired value. This allowed us to correct for losses due to molecule formation and three-body recombination [1].

Once we had the Fermi cloud at the intended bias field, we imparted momentum in the x direction to half of the cloud and in the $-x$ direction to the other half and observed them scatter as they moved through each other and separated. To impart the momentum, we used a double pulse sequence [10] of a near resonant 1-d retro-reflected optical lattice. The pulse sequence was optimized to transfer most of the atoms into the first two excited states of the lattice, giving them $\pm 2k_r$ of momentum, where k_r is the recoil momentum of the lattice. Since the initial Fermi gas had a wide momentum spread (in contrast to a BEC, which has a very narrow momentum spread), and the lattice pulsing is a momentum dependent process, not all the atoms were successfully transferred into the 1st excited band of the lattice. We optimized our pulse times to minimize the number of atoms that remain in the zero momentum band of the lattice, but were not able to eliminate them completely. The optimized pulse times are $23\mu s$ for the first square pulse, $13\mu s$ off interval, and $12\mu s$ for the second square pulse.

We then released the atoms from the trap and allowed 1ms for the two opposite momentum states within the cloud to pass through each other, scattering on the way. For the data taken coming from below the Feshbach resonance, we then simply ramped down the field and imaged the atoms. For the data taken coming from above the Feshbach resonance, we ramped the field back up through the resonance to recover any molecules that were created when the field was ramped from the attractive to the repulsive side of the resonance, and then quickly ramped the field back down and imaged the atoms. We use an imaging pulse of $40\mu s$.

The total time from the moment the atoms were released from the trap to when they were imaged, known as the time of flight, was 6.784 ms. In such an image, the location of each atoms is determined by how far it traveled in that time of flight, which is determined by its initial momentum when it was released from the trap. Therefore, this technique measures the momentum and not the position distribution of the atoms.

3.2. Methods

We first corrected each image for recoil induced detuning using the simulation described above. We simulated a look-up table of predicted optical depths as a function of atomic column density and probe intensity. From our two absorption images we knew the probe intensity and optical depth for each pixel. We then used the simulated look-up table in an inverted fashion to deduce the atomic column density. An example of the effect of this correction procedure is shown in Fig. 11. To improve the signal and compensate for our shot to shot number fluctuations, we took 15 equivalent images for each data point and, after correcting, added them together.

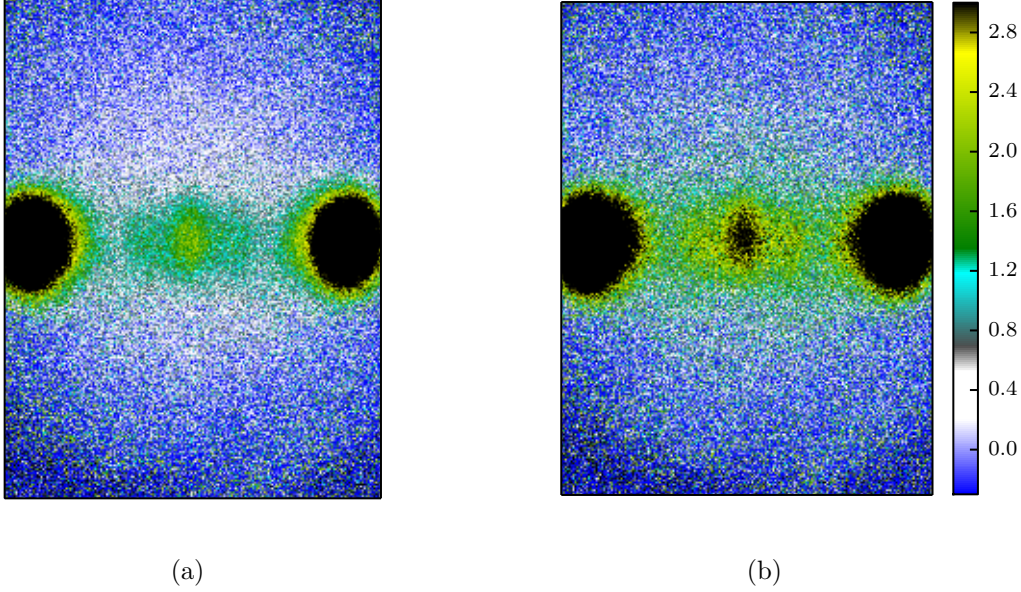


Figure 11. An example of our absorption image after 6.784ms time of flight. The 1-D lattice is along the horizontal direction at the center of our images. The two large clouds on the left and right are the atoms in the $\pm 2k_r$ momentum orders that passed through each other unscattered. The smaller cloud in the center is the atoms that remained in the lowest band of the lattice after pulsing, and thus obtained no momentum. The thin spread of atoms around these clouds is the atoms that underwent scattering. This image was taken coming from below the Feshbach resonance at 20.07 mT. a. Raw optical density b. Optical density of the same image after correcting for recoil induced detuning

Once we acquired scattering images at a sufficient number of field values, we wanted to extract the fraction of atoms that underwent a single scattering event as a function of the bias field. We focused our attention on single-scattered atoms because, once an atom has scattered multiple times it is hard to determine precisely how many times it scattered, and therefore hard to deduce the scattering cross section. An atom that underwent a single scattering event, however, is easily identified, as two atoms that scatter elastically will keep the same amplitude of momentum in an arbitrary direction. Therefore, an atom traveling at $2k_r$ to the right that collides with an atom traveling at $2k_r$ to the left will acquire a momentum of $2k_r$ in some direction, and in a time of flight image such atoms will lie in a spherical fashion around the center of mass - the scattering halo, pictured in Fig. 12a.

Absorption images captured the integrated column density along z , a projected 2-d atomic distribution. In order to extract the radial dependence of the 3-d distribution from the 2-d image, we performed a standard inverse Abel transform. The inverse Abel transform assumes a cylindrical symmetry, which was present in our case, with the axis of symmetry along x , defined by the lattice. We thus obtained the atomic distribution as a function of r , the radial distance from the scattering center, and θ , the angle between

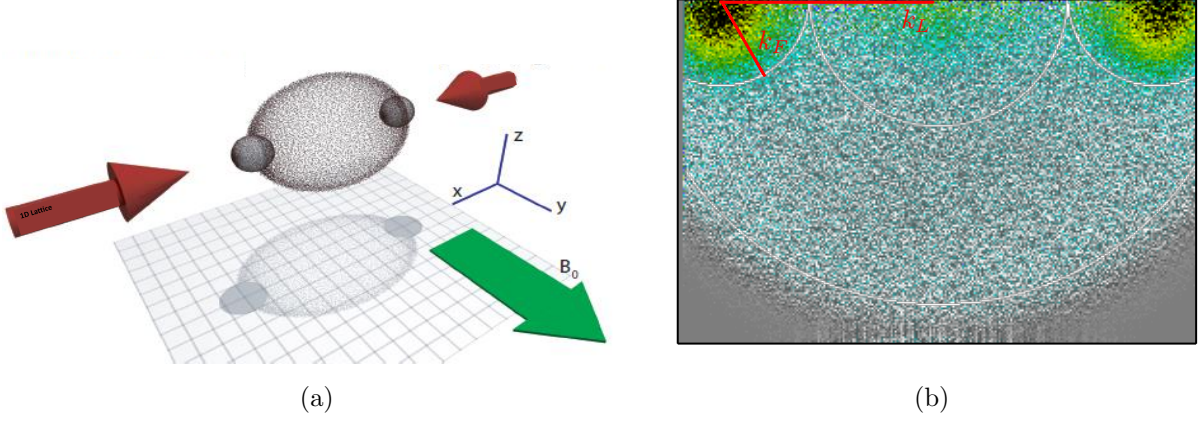


Figure 12. a. Our experimental setup. After time of flight, the two clouds traveling in opposite x directions have separated and the atoms that underwent a single scattering event were evenly distributed in a scattering halo around the unscattered clouds. An absorption image captured the shadow the clouds cast onto a 2-d plane. b. Inverse Abel transformed image. The atoms within the Fermi radius k_F of each unscattered cloud center are in the unscattered region and counted towards the total unscattered number. The atoms outside the radius $k_r - k_F$ but inside $k_r + k_F$ but outside the unscattered region are counted towards the number of single scattered atoms.

r and symmetry axis x , integrated over ϕ , the azimuthal angle around the x axis.

We then extracted the number of atoms that went through a single scattering event N_{scat} , as a fraction of the total atom number N_{tot} , for each bias magnetic field value from the transformed images, as shown in Fig. 12b. We obtained the unscattered atom number by counting the number of atoms in the two unscattered clouds. We obtained the number of atoms that underwent a single scattering event by counting the number of atoms outside the Fermi radius of the unscattered clouds, but inside the arc created by rotating the Fermi momentum k_F radius around the original center of the cloud. The total atom number in the image was the sum of those two.

We then used our data to deduce the resonant field value B_0 and width of the resonance Δ , the parameters in Eq. (1). To do this, we fit our data to a model. Since we were in the low energy regime, the scattering cross-section was given by $\sigma = 4\pi a^2$.

One way to think about the scattering cross-section σ is that the probability P_{scat} that a single particle will get scattered when incident on a cloud of atoms with a surface density of $\frac{N}{A}$ is given by $P_{scat} = \sigma \frac{N}{A}$. If this experiment is repeated 1000 times, the number of times the atom will get scattered is expected to be $N_{scat} = 1000\sigma \frac{N}{A}$. In our case, half the initial cloud, with atoms number $N_{tot}/2$, is incident on the other half of the initial cloud, again with $N_{tot}/2$ atoms. Thus, the number of scattered atoms should be given by $N_{scat} = \frac{N_{tot}}{2}\sigma \frac{N_{tot}}{2} = \sigma \frac{N_{tot}^2}{4A}$, where A is the cross-sectional area of the cloud. Assuming A is constant for all our data, we can absorb the factor of $4A$ into our definition of a_{bg} , along with the 4π , to obtain

$$\frac{N_{scat}}{N_{tot}^2} = \tilde{a}_{bg}^2 \left(1 - \frac{\Delta}{B - B_0}\right)^2 + C. \quad (15)$$

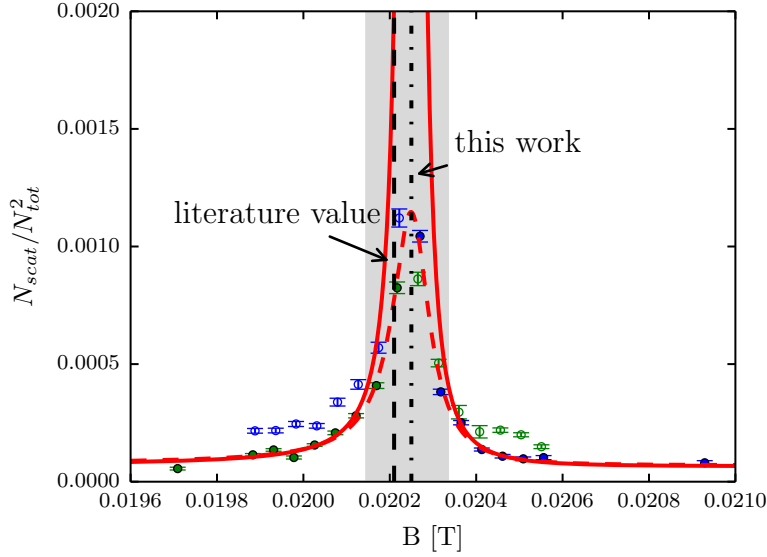


Figure 13. Normalized scattered population plotted versus bias field B . Green dots represent data taken coming from below the resonance, and blue dots represent the data taken coming from above the resonance. Red is the line of best fit, where data coming from above the resonance was used above the resonance and data coming from below the resonance was used below the resonance to create the fit. The regime where the scattering length is likely large enough for the atoms to behave hydrodynamically is shaded in gray. Data points in that region were not used in the fit, as there the assumption $\sigma\rho \ll 1$, where ρ is the atom number per unit area, is no longer valid. Values for the resonant field B_0 from literature and as found in this work are indicated.

We found that our imaging noise skewed towards the positive, giving rise to a small background offset. We accounted for this in our fit by including a constant offset parameter C .

3.3. Results

Our final data is presented in Fig. 13. The red line is a best fit of the model given in Eq. (15). The fit parameters we extracted are $\tilde{a}_{bg} = 1.48e - 3$, $\Delta = 1.0(1)$ mT, $B_0 = 20.247(2)$ mT, and $C = 9.00e - 5$. The error bars on the fitted data were obtained solely from photon shot noise of both absorption images propagated through our analysis. The accepted values for the ^{40}K s-wave Feshbach resonance for the $|9/2, -9/2\rangle$ and $|9/2, -7/2\rangle$ states are $B_0 = 20.210(7)$ mT and $\Delta = 0.78(6)$ mT. The difference in our measurement may be a result of scattering with the center cloud that recieved no momentum kick, a process that was not taken into account by our analysis.

4. Conclusion

We studied the effects of recoil-induced detuning effects on absorption images and found an optimal imaging time of $40\mu\text{s}$ for ^{40}K atoms for noise minimization after corrections. We use these results to observe s-wave scattering halos of the Fermi gas around the Feshbach resonance and directly verify the resonance location and width. Our analysis can be used in any absorption imaging applications where signal to noise minimization is critical. We performed a new kind of measurement of the resonant magnetic field and with of a Feshbach resonance.

Acknowledgments

We thank Marcell Gall for helpful discussions. This work was partially supported by the AROs Atomtronics MURI, by the AFOSRs Quantum Matter MURI, NIST, and the NSF through the PFC at the JQI. B.K.S. is a NIST-NRC Postdoctoral Research Associate. L.M.A. was supported by the NSF GRFP.

References

- [1] Cheng Chin, Rudolf Grimm, Paul Julienne, and Eite Tiesinga. Feshbach resonances in ultracold gases. *Rev. Mod. Phys.*, 82:1225–1286, Apr 2010.
- [2] Bo Gao. Analytic description of atomic interaction at ultracold temperatures. ii. scattering around a magnetic feshbach resonance. *Phys. Rev. A*, 84:022706, Aug 2011.
- [3] Lindsey J. LeBlanc. *Exploring many-body physics with ultracold atoms*. PhD thesis, University of Toronto, 2011.
- [4] M. Lysebo and L. Veseth. *Ab initio* calculation of feshbach resonances in cold atomic collisions: *s*- and *p*-wave feshbach resonances in $^6\text{Li}_2$. *Phys. Rev. A*, 79:062704, Jun 2009.
- [5] C. Monroe, E. Cornell, C. Sackett, C. Myatt, and C. Wieman. Measurement of cs-cs elastic scattering at $T = 30\mu\text{K}$. *Phys. Rev. Lett.*, 70:414–417, Jan 1993.
- [6] K. M. O’Hara, S. L. Hemmer, M. E. Gehm, S. R. Granade, and J. E. Thomas. Observation of a strongly interacting degenerate fermi gas of atoms. *Science*, 298(5601):2179–2182, 2002.
- [7] C. Regal and D. Jin. Measurement of positive and negative scattering lengths in a fermi gas of atoms. *Phys. Rev. Lett.*, 90:230404, Jun 2003.
- [8] Cindy Regal. *Experimental realization of BCS-BEC crossover physics with a Fermi gas of atoms*. PhD thesis, JILA, 2005.
- [9] G. Reinaudi, T. Lahaye, Z. Wang, and D. Guéry-Odelin. Strong saturation absorption imaging of dense clouds of ultracold atoms. *Opt. Lett.*, 32(21):3143–3145, Nov 2007.
- [10] Saijun Wu, Ying-Ju Wang, Quentin Diot, and Mara Prentiss. Splitting matter waves using an optimized standing-wave light-pulse sequence. *Phys. Rev. A*, 71:043602, Apr 2005.